ChemPubSoc Europe

DOI: 10.1002/cctc.201801578

CHEMCATCHEM Full Papers

Engineering Nanoceria for Enhanced Peroxidase Mimics: A Solid Solution Strategy

Wenjing Guo[+],[a] Mian Zhang[+],[a] Zhangping Lou[+],[a] Min Zhou,[a] Peng Wang,*[a, b] and Hui Wei*[a, c]

Nanoceria has been developed as a biocompatible and robust enzyme mimic (called ceria nanozyme) and applied in bioanalysis and therapeutics. However, its catalytic activity such as peroxidase mimic is still moderate, which in turn has limited its promising applications. To tackle this issue, herein we reported an effective strategy to modulate the peroxidase mimicking activity of nanoceria by doping transition metals. We discovered that doping of the first row of transition metals (*i.e.*, Mn, Fe, Co, Ni, and Cu) modulated the activity of nanoceria and with the same doping ratio the activities followed the below order: $Mn_1Ce_{10} > Co_1Ce_{10} > Fe_1Ce_{10} > Cu_1Ce_{10} > CeO_2 > Ni_1Ce_{10}$. By further varying the Mn/Ce ratio, Mn_1Ce_5 with the highest peroxidase mimicking activity was obtained (13-fold higher compared with the pristine CeO_2). Meanwhile we found that the homogenous doping of Mn into the nanoceria matrix without phase segregation ensured the formation of Mn_1Ce_5 solid solution. From our experiments and discussion, we concluded that the surface oxygen (O_β) and the synergistic effect between Ce and Mn played key roles in the enhancement of Mn_1Ce_5 peroxidase mimicking activity. This study not only demonstrates that Mn-doped nanoceria exhibits higher active peroxidase mimics but also provides a promising strategy to modulate the catalytic activity of nanozymes.

1. Introduction

Nanoceria (CeO_2), as one of the most important nanocatalysts, has been widely explored for a variety of industrial applications, including carbon monoxide oxidation, nitrogen oxide conversion, and water splitting.[1] Recently, it has attracted enormous interests in mimicking various natural enzymes, such as superoxide dismutase (SOD), catalase, oxidase, peroxidase, phosphatase, *etc.*[2] Among the developed enzyme mimicking nanomaterials (*i.e.*, nanozymes),[3] ceria nanozymes are notable in several aspects, such as their multiple enzyme mimicking activities, remarkable robustness, and excellent biocompatibility. Therefore, ceria nanozymes have been utilized for broad applications, ranging from glucose detection and immunoassay to ischemic stroke protection and anti-biofouling.[2b,3l,v,4]

Despite of the substantial progress, the catalytic activities of ceria nanozymes are still moderate. Till now, numerous strategies have been developed to modulate the activities of nanozymes.[5] Among them, a few have been proposed to improve the catalytic activities of ceria nanozymes. For example, the SOD mimicking activity of nanoceria was significantly enhanced through electron transfer.[6] The peroxidase mimicking activities of nanoceria were tuned by controlling the nanomaterials' morphology and structure.[2h] We have showed that the oxidase mimicking activities of nanoceria could be modulated by using small molecules.[7] With the success of the above developed strategies, more interests are focused on searching for effective strategies to enhance the enzyme mimicking activities of nanoceria.

On the other hand, recent studies showed that the doping of redox active aliovalent transition metals into the matrix of nanoceria to form $M_xCe_{1-x}O_{2-y}$ solid solution, which significantly enhanced the catalytic activities of nanoceria towards carbon monoxide and hydrocarbon oxidation.[1b,c,8] The enhancement was attributed to the increased concentration and migration of oxygen vacancies.[9] We reason that such transition metal-doping could also be an effective strategy for modulating the redox enzyme mimicking activities of nanoceria since similar oxygen species are involved in the biomimetic catalysis. Encouragingly, a few recent studies indicated that it was possible to improve the catalytic activities of ceria nanozymes by doping with Mo, Fe, or Zr.[2c,5c,10] However, no systematic studies have been carried out to elucidate the mechanistic roles of the doped metal in the enzyme mimicking activities.

To fill this gap, herein we showed the peroxidase mimicking activity of nanoceria could be effectively modulated by doping

[a] *W. Guo,[+] M. Zhang,[+] Z. Lou,[+] M. Zhou, Prof. P. Wang, Prof. H. Wei*
College of Engineering and Applied Sciences
Nanjing National Laboratory of Microstructures
Jiangsu Key Laboratory of Artificial Functional Materials
Nanjing University
Nanjing, Jiangsu, 210093 (P.R. China)
E-mail: wangpeng@nju.edu.cn
weihui@nju.edu.cn
Homepage: http://weilab.nju.edu.cn
[b] *Prof. P. Wang*
Research Center for Environmental Nanotechnology (ReCENT)
Nanjing University
Nanjing, Jiangsu, 210023 (P.R. China)
[c] *Prof. H. Wei*
State Key Laboratory of Analytical Chemistry for Life Science and State Key Laboratory of Coordination Chemistry
School of Chemistry and Chemical Engineering
Collaborative Innovation Center of Chemistry for Life Sciences
Nanjing University
Nanjing, Jiangsu 210023 (P.R. China)
[+] *These authors contributed equally to this work.*

Supporting information for this article is available on the WWW under https://doi.org/10.1002/cctc.201801578

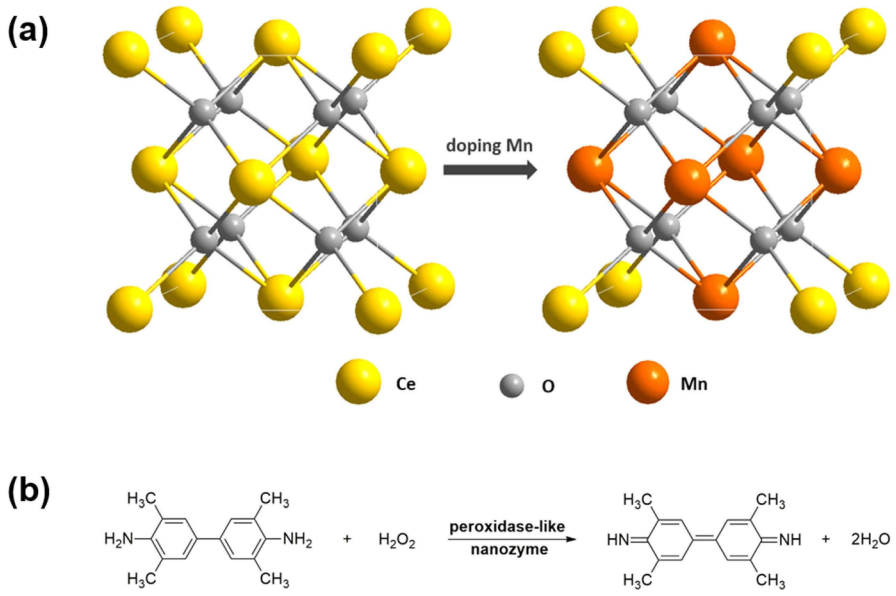

Figure 1. (a) Schematic illustration of engineering nanoceria by transition metal doping for enhanced peroxidase mimics. (b) Peroxidase-like nanozyme catalyzes the oxidation of TMB with hydrogen peroxide.

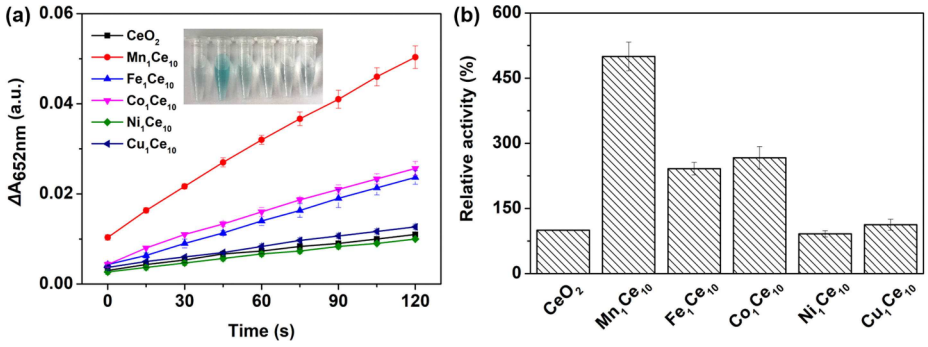

Figure 2. (a) Time evolution of calibrated absorbance at 652 nm (ΔA_{652}) during the catalytic oxidation of TMB with 500 μM H_2O_2 in pH 4.5 acetate buffer at 25 °C, in the presence of 10 μg/mL of CeO_2, Mn_1Ce_{10}, Fe_1Ce_{10}, Co_1Ce_{10}, Ni_1Ce_{10}, and Cu_1Ce_{10} nanozymes. Inset: photo of each reaction system containing nanozymes in the above order. (b) Normalized peroxidase mimicking activities of CeO_2 and M-doped CeO_2 nanozymes. The activity of CeO_2 was defined as 100%. Each error bar shows the standard deviation of three independent measurements, the error bar of CeO_2 is too narrow to be seen.

the first row of transition metals (*i.e.*, Mn, Fe, Co, Ni, and Cu) (Figure 1). Among the doped nanoceria, we found that Mn-doped nanoceria solid solution exhibited the highest catalytic activity. Further systematic studies revealed that surface oxygen (O_β) and the synergistic effect between Ce and Mn played critical roles in the enhancement of nanoceria peroxidase mimicking activities.

2. Results and Discussion

2.1. Transition Metal Doped Nanoceria as Peroxidase Mimics

Several representative first row of transition metals (*i.e.*, Mn, Fe, Co, Ni, and Cu) were used to modulate the peroxidase mimicking activity of nanoceria. CeO_2 and transition metal-doped CeO_2 nanozymes were synthesized *via* a low-temperature hydrothermal method. Citrate was then used to treat the as-prepared nanozymes, which made the nanozymes more water soluble and more stable (Figure S1). TEM and XRD techniques were used to characterize the morphology and the phase composition of CeO_2 and doped CeO_2. As shown in Figure S2, both CeO_2 and doped CeO_2 had similar sizes (around 3–5 nm) and irregular shapes. As shown in Figure S3, the XRD patterns of all the doped CeO_2 matched well with the standard cubic fluorite structure of ceria (JCPDS card No. 43-1002). Moreover, since no multiple phases were observed, demonstrating the formation of phase-pure solid solution of $M_xCe_{1-x}O_{2-\delta}$.

The peroxidase mimicking activities of the doped CeO_2 nanozymes were then evaluated by monitoring the catalytic oxidation of TMB with the corresponding nanozyme in the presence of H_2O_2. As shown in Figure 2a, compared with CeO_2, Fe_1Ce_{10}, Co_1Ce_{10}, and Mn_1Ce_{10} showed faster kinetic rates while Ni_1Ce_{10} and Cu_1Ce_{10} showed slower or similar kinetic rates.

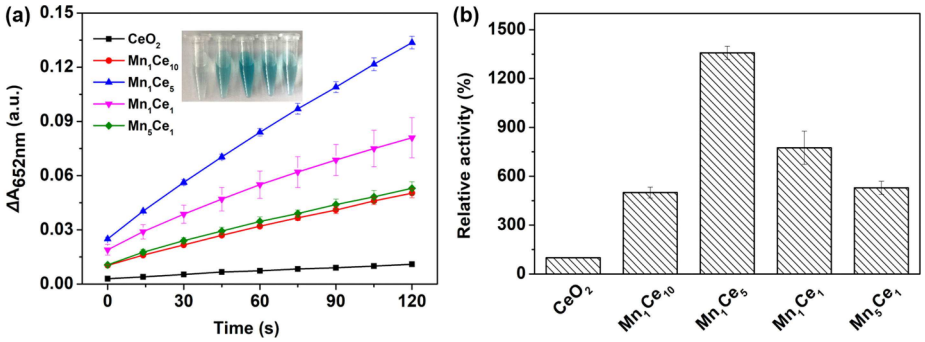

Figure 3. (a) Time evolution of calibrated absorbance at 652 nm (ΔA_{652}) during the catalytic oxidation of TMB with 500 μM H_2O_2 in pH 4.5 acetate buffer at 25 °C, in the presence of 10 μg/mL of CeO_2, Mn_1Ce_{10}, Mn_1Ce_5, Mn_1Ce_1, and Mn_5Ce_1 nanozymes. Inset: photo of each reaction system containing nanozymes in the above order. (b) Normalized peroxidase mimicking activities of CeO_2 and Mn-doped CeO_2 nanozymes. The activity of CeO_2 was defined as 100%. Each error bar shows the standard deviation of three independent measurements, the error bar of CeO_2 is too narrow to be seen.

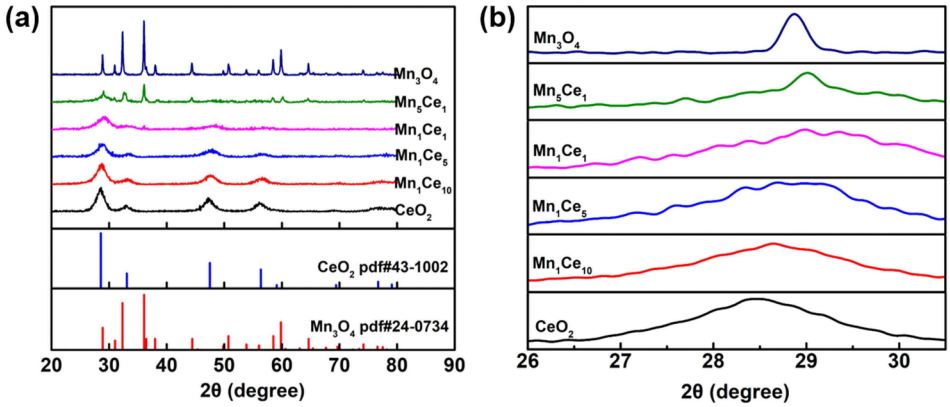

Figure 4. (a) XRD patterns of CeO_2, Mn_3O_4, and Mn-doped CeO_2 with different Mn to Ce ratios. The red and blue lines at the bottom mark the reference patterns of CeO_2 and Mn_3O_4 from the JCPDS database, respectively. (b) Enlarged patterns around (111) plane of CeO_2.

Further analysis showed that the peroxidase mimicking activities of the doped CeO_2 exhibited the following order: $Mn_1Ce_{10} > Co_1Ce_{10} > Fe_1Ce_{10} > Cu_1Ce_{10} > CeO_2 > Ni_1Ce_{10}$ (Figure 2b). Since the Mn doping promoted the catalytic activity in the most extent, we then focused on the Mn-doped CeO_2 nanozymes to elucidate the mechanisms responsible for the enhanced catalytic activity.

2.2. Mn-Doped Nanoceria as Peroxidase Mimics

Having identified Mn as the best doping transition metal for enhancing the peroxidase-like activity of nanoceria, we prepared a series of Mn-doped CeO_2 nanozymes by varying the Mn to Ce ratios and studied their activities. As shown in Figure 3, with the increasing Mn content, the activity of Mn-doped CeO_2 nanozymes reached the highest value when the ratio of Mn/Ce was 1:5, later with the ratio above 1:5 the activities showed some decrease but still higher than the pristine CeO_2. The obtained Mn_1Ce_5 nanozyme exhibited the highest peroxidase-like activity, which was more than 13-fold higher compared with CeO_2.

Further control experiments were also performed to confirm the intrinsic peroxidase-like activity of Mn_1Ce_5 nanozyme. First, in Figure S4, after incubating at 37 °C for 10 min, the reaction system including Mn_1Ce_5 nanozyme, TMB and H_2O_2 showed a dark blue color. In contrast, nearly no color changes were seen with TMB alone or TMB combined with H_2O_2. It is worthy to noticed that the reaction system with TMB and Mn_1Ce_5 also showed slight color change, which was contributed to the oxidase-like activity of Mn_1Ce_5. Second, the peroxidase-like activity of Mn_1Ce_5 was also evaluated using other typical substrate likes ABTs and OPD. As shown in Figure S5, obvious color changes were observed after adding Mn_1Ce_5 nanozyme. All the above control experiments demonstrating the intrinsic peroxidase-like activity of Mn_1Ce_5 nanozyme.

To understand the Mn/Ce ratio dependent activity of Mn-doped CeO_2 nanozymes, their crystalline structures were first investigated by XRD. Figure 4a showed XRD patterns of CeO_2, Mn_3O_4, and Mn-doped CeO_2 with different Mn/Ce ratios. For CeO_2, the characteristic peaks at $2\theta = 28.5°$, 33.1°, 47.5°, and 56.3° corresponding to (111), (200), (220), and (311) reflection planes were observed, which indicated the cubic structure of CeO_2. For Mn_3O_4, the characteristic peaks could be assigned to

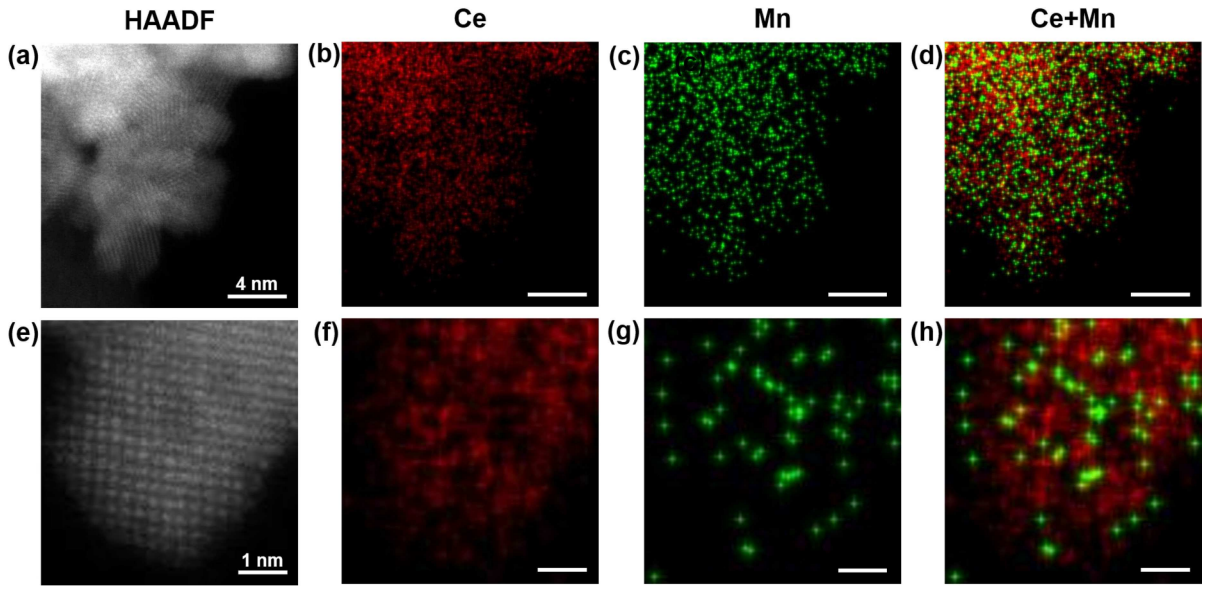

Figure 5. (a, e) STEM-HAADF images of several and single Mn_1Ce_5 nanoparticles. (b-d, f-h) The elemental maps of Ce, Mn, and overlay.

the tetragonal hausmannite structure (see SI for detailed assignments).

As shown in Figure 4a, upon doping of Mn into the CeO_2 matrix, the crystalline structure started showing the tetragonal hausmannite structure of Mn_3O_4, and finally dominant tetragonal hausmannite structure of Mn_3O_4 formed. Compared with pure CeO_2, Mn_1Ce_{10} and Mn_1Ce_5 still had the cubic structure of CeO_2 but their diffraction peaks showed a clear shift towards higher Bragg angles in the range of 27.0-30.0° (Figure 4b). The shift could be attributed to the incorporation of smaller Mn ions into the lattice of Ce (ionic radii: Mn^{2+}: 0.083 nm; Mn^{3+}: 0.065 nm; Mn^{4+}: 0.053 nm; Ce^{3+}: 0.114 nm; Ce^{4+}: 0.097 nm).[6] As the ratio of Mn/Ce reached 1:1, the diffraction pattern showed a clear representative peak of Mn_3O_4 with tetragonal hausmannite structure (*i.e.*, the peak at 36.1°). For Mn_5Ce_1, more pronounced peaks of Mn_3O_4 appeared while the peaks of CeO_2 nearly disappeared.

The crystalline structures were further analyzed by TEM imaging (Figures S7 and S8). For CeO_2 and Mn_1Ce_{10}, the interplanar spacing was predominated with 0.315/0.316 nm, which could be attributed to the stable (111) plane of cubic CeO_2. For Mn_1Ce_5, the interplanar spacing was shrunk to 0.308 nm. This result was consistent with XRD data. However, for Mn_1Ce_1 and Mn_5Ce_1, the inter-planar spacing increased to 0.312 nm and 0.317 nm, respectively. These could be assigned to the (112) plane of tetragonal hausmannite structure Mn_3O_4. The increase was reasonable since phase segregation was observed for both Mn_1Ce_1 and Mn_5Ce_1 (see the XRD results above). For Mn_3O_4, an interplanar spacing of 0.212 nm was observed, which was attributed to the (220) plane.

For both Mn_1Ce_{10} and Mn_1Ce_5, the absence of phase segregation as well as the XRD peak shift and lattice shrink indicated the formation of solid solution after doping of smaller size Mn ions into CeO_2.

Since Mn_1Ce_5 had the highest peroxidase mimicking activity, its solid solution phase was further investigated by analyzing its element distribution with STEM-EDS mapping. As shown in Figure 5a–d, homogeneous dispersion of Ce and Mn within Mn_1Ce_5 nanoparticles was observed. The well-dispersion of Ce and Mn was further confirmed by imaging a single Mn_1Ce_5 nanoparticle (5e–h). Figure 5d and 5 h also revealed that Mn atoms entered into the lattice structure of CeO_2 by replacement of Ce atoms. Moreover, no segregation was observed. The STEM-EDS mapping analysis further confirmed the formation of homogeneous Mn_1Ce_5 solid solution.

2.3. XPS Analysis

To get further insights into the Mn/Ce ratio dependent activity of Mn-doped CeO_2 nanozymes, their composition and oxidation state were analyzed by XPS analysis. The survey spectrum in Figure 6a confirmed the presence of Ce, Mn, and O elements in the Mn-doped CeO_2 nanozymes.

As shown in Figure 6b, five pairs of spin-orbit coupling of Ce 3d spectra could be assigned to two orbits $3d_{5/2}$ and $3d_{3/2}$, labeled as v and u, respectively. Among them, v, v″, v‴, u, u″, and u‴ were attributed to Ce^{4+} while v_0, v′, u_0, and u′ were attributed to Ce^{3+}.[11] These results demonstrated that the Ce^{4+} and Ce^{3+}co-existed in the Mn-doped CeO_2 and Ce^{4+} was dominant. As shown in Figure 6d, the fraction of Ce^{3+} decreased with the increasing content of Mn, which was not well correlated with the catalytic activity. So we summarized that Ce^{3+} was not the main factor for enhancement of activity. Apart from the valence of Ce, there was another important factor (*i.e.*, oxygen species) could be worth to study. Therefore, we further analyzed the oxygen species.

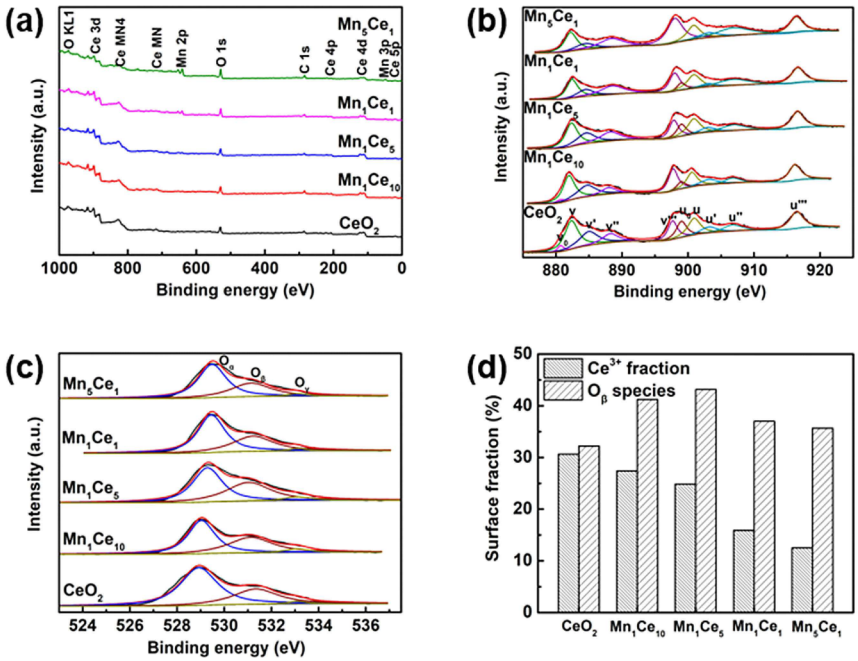

Figure 6. (a) XPS survey scan, (b) Ce 3d core level XPS spectra, (c) O 1s core level XPS spectra, (d) surface fraction of Ce^{3+} and O_β species of different nanozymes.

Figure 6c showed the O 1s spectra at the binding energy of 526.0–534.0 eV, which was broad with shoulder peaks. The curves were deconvoluted into three peaks, which were attributed to the lattice oxygen (528.9–529.5 eV; O^{2-}; O_α), the surface oxygen species (531.0–531.5 eV; O_2^-, O_2^{2-}, O^-; O_β), and the chemisorbed water and/or carbonates (533.1 eV; O_γ), respectively.[11a] Compared with CeO_2, the binding energy of the O1s species shifted to higher binding energy value after Mn doping, which was probably due to the environment change of oxygen due to the interaction between the Ce–O and Mn–O.[11a] It is known that O_β from defective sites plays an important role in most of catalysis processes.[9b, 12] Compared Figure 6d with Figure 3b, it clearly showed that Mn_1Ce_5 with the most abundant O_β (*i.e.*, 43.2%) had the highest peroxidase mimicking activity. Moreover, the abundance of O_β of CeO_2 and Mn-doped CeO_2 had a strong correlation with the peroxidase mimicking activity. Interestingly, a similar correlation was also found in the other transition metal doped nanoceria (Figure S10). These results indicated the O_β played a dominant role in the peroxidase mimicking activity of CeO_2 and Mn-doped CeO_2. As shown in Figure S11, the mixture of CeO_2 and Mn_3O_4 nanoparticles showed much lower activity than the same amount of Mn_1Ce_5, demonstrating the synergistic effect between Ce and Mn with more active oxygen species on the catalytic activity.

2.4. Kinetics Analysis

After optimizing the reaction pH and temperature (Figure S12), the steady-state kinetics assays of Mn_1Ce_5 and CeO_2 were performed (Figures S13 and S14). Michaelis-Menten constants (K_m) and maximum initial velocity (V_{max}) were summarized in Table S2. Compared with CeO_2, the lager K_m value of Mn_1Ce_5 with H_2O_2 indicated the weaker affinity of Mn_1Ce_5 towards H_2O_2. However, a smaller K_m value of Mn_1Ce_5 with TMB was observed, indicating the stronger affinity of Mn_1Ce_5 towards TMB. Moreover, the V_{max} values of Mn_1Ce_5 for TMB and H_2O_2 were 2.5- and 30-fold higher than that of CeO_2, respectively. These results confirmed that catalytic efficiency of CeO_2 could be greatly enhanced by Mn doping.

2.5. Superior Peroxidase Mimicking Activity of Mn_1Ce_5

To demonstrate the superior peroxidase mimicking activity of Mn_1Ce_5, we compared its pH and thermal stability with several representative peroxidase mimicking nanozymes (*i.e.*, Au, Fe_3O_4, and $Cu(OH)_2$). As shown in Figures S15, Mn_1Ce_5 exhibited better pH and thermal stability than other nanozymes. As shown in Figures S16, Mn_1Ce_5 also exhibited better pH and thermal stability than natural peroxidases (such as horseradish peroxidase).

Recently, it was reported that $Cu(OH)_2$ nanocages exhibited comparable catalytic activity as natural horseradish peroxidase.[13] Therefore, we synthesized $Cu(OH)_2$ nanocages (Figures S17) and compare their peroxidase mimicking activity with Mn_1Ce_5 nanozyme (Figures S18). Encouragingly, Mn_1Ce_5 exhibited 9-fold higher activity than $Cu(OH)_2$ nanocages, demonstrating the superior peroxidase mimicking activity of Mn_1Ce_5.

3. Conclusion

In summary, we developed an effective solid solution strategy to modulate the peroxidase mimicking activity of nanoceria by doping transition metals. We showed that the activity of nanoceria was significantly enhanced after Mn doping. We further revealed that homogenous Mn_1Ce_5 solid solution with the highest Mn content exhibited the highest peroxidase mimicking activity. Systematic mechanism study indicated that both the surface oxygen (O_β) and the synergistic effect between Ce and Mn played key roles in the peroxidase mimicking activity of the Mn doped nanoceria. The obtained nanozymes were also advantageous over natural enzymes and other typical peroxidase mimics in several aspects, such as lower cost, higher stability, and good biocompatibility. This study not only demonstrates Mn doped nanoceria as promising peroxidase mimics but also provides an effective and facile strategy for modulating the catalytic activity of nanozymes. It may also help to understand the catalytic mechanism of ceria-based nanozymes.

Experimental Section

Chemicals and materials: Cerium (III) nitrate hexahydrate ($Ce(NO_3)_3 \cdot 6H_2O$, 99%), manganese acetate ($Mn(CH_3COO)_2$, 99%), ethylene glycol (99%), ammonium hydroxide ($NH_3 \cdot H_2O$, AR), trisodium citrate dehydrate (99%), hydrogen peroxide (H_2O_2, AR), and acetone (AR) were obtained from Sinopharm Chemical Reagent Co., Ltd. Cobalt acetate ($Co(CH_3COO)_2$, 99.5%), iron nitrate ($Fe(NO_3)_3$, 98.5%), 3,3′,5,5′-tetramethylbenzidine dihydrochloride hydrate (TMB, 98%), and glycine (ACS, 98.5%) were from Aladdin Chemical Reagent Co., Ltd. Sodium acetate (CH_3COONa, 99%) and disodium hydrogen phosphate (Na_2HPO_4, 99%) were from Nanjing Chemical Reagent Co., Ltd. Nickel nitrate ($Ni(NO_3)_2$, 98.0%) was from Guangdong Guanghua Sci-Tech Co., Ltd. Cupric acetate ($Cu(CH_3COO)_2$, 99.0%) was from Shanghai Xinbao Fine Chemical Factory. All chemical reagents were used as received without further purification. All aqueous solutions were prepared with deionized water (18.2 MΩ·cm, Millipore).

Instrumentation: Transmission electron microscopy (TEM) images were obtained on a FEI Tecnai G2 F20S-TWIN microscope at an acceleration voltage of 200 kV. Scanning TEM-high-angle annular dark field (STEM-HAADF) images and energy-dispersive spectroscopy (EDS) elemental mappings were acquired using a FEI Titan^3 G2 60–300 microscope, operated at an accelerating voltage of 60 kV, equipped with double aberration correctors and Super-X EDS detectors. Powder X-ray diffraction (XRD) patterns were collected on a Thermo Fisher Scientific XTRA diffractometer in the 2θ range of 20–85° by using Cu Kα radiation. X-ray photoelectron spectroscopy (XPS) was obtained using a PHI 5000 VersaProbe (Ulvac-Phi, Japan). The C 1s binding energy 284.8 eV was used as a reference to calibrate the binding energy of other elements. UV-visible absorption spectra were recorded using a TU-1900 spectrophotometer (Beijing Purkinje General Instrument Co. Ltd., China). The contents of Ce and Mn were measured by an inductive coupled plasma optical emission spectrometer (ICP-OES) (OPTIMA 530DV, PerkinElmer).

Synthesis of $MxCe_{1-x}O_2$ nanoparticles: $M_xCe_{1-x}O_{2-\delta}$ (M=Mn, Fe, Co, Ni, and Cu) nanoparticles were prepared as follows (see sample names in Table S1).[12b] Cerium nitrate (1.16 mM, 503.70 mg) and appropriate amount transition metal acetate (or transition metal nitrate) were dissolved in 20 mL water-ethylene glycol (1:1) mixed solvent. The reaction solution was bath-heated under stirring until the temperature reached 60 °C. Then, 3.2 mL $NH_3 \cdot H_2O$ was quickly added to the reaction solution. After 3 h vigorously stirring at 60 °C, the corresponding product was obtained, which was washed multiple times with water. (Note: pure CeO_2 was yellowish.)

To enhance the water solubility of the above-synthesized nanoparticles, these obtain nanoparticles were further treated with citrate according to our reported protocol.[7] Briefly, the nanoparticles were first precipitated *via* centrifugation. Then, 10 mL water and 2 mL sodium citrate solution (60 mg/mL) were added. After 10 min sonication, the solution was further centrifuged (10000 r/min, 10 min) to remove free citrate. To obtain better dispersed and highly concentrated nanoparticles, the citrate treatment could be repeated *via* adding 10 mL sodium citrate solution (60 mg/mL) into the precipitate, which was followed by sonicating and centrifugation. The citrate modified nanoparticles should be highly transparent, which were stored for further studies.

Evaluation of the peroxidase mimicking activity of the nanozymes: The peroxidase mimicking activity of the as-prepared nanozymes was measured by using a peroxidase chromogenic substrate TMB as the reporter. Typically, 20 μL of 25 mM H_2O_2 and 20 μL of 25 mM TMB were added to 940 μL of reaction buffer. After 1 min vortexing, 20 μL of 0.5 mg/mL nanozymes was quickly added. The mixed solution was immediately used for absorption spectroscopy measurement by monitoring the absorbance value at 652 nm (A_{652}) with a UV-visible spectrophotometer. (See Figure S6 and associated discussion about details for the peroxidase-mimicking activities calculations.)

Author Contributions

The manuscript was written through contributions of all authors. All authors have given approval to the final version of the manuscript.

Notes

The authors declare no competing financial interest.

Acknowledgements

This work was supported by National Natural Science Foundation of China (21722503, 21874067, 11474147 and 11874199), 973 Program (2015CB659400), PAPD program, Shuangchuang Program of Jiangsu Province, Open Funds of the State Key Laboratory of Analytical Chemistry for Life Science (SKLACLS1704), Open Funds of the State Key Laboratory of Coordination Chemistry (SKLCC1819), Fundamental Research Funds for the Central Universities (021314380103), Thousand Talents Program for Young Researchers, and National Basic Research Program of China (2015CB654901). We thank Xingfa Gao, Jia Yao, and Faheem Muhammad for insightful discussions.

Conflict of Interest

The authors declare no conflict of interest.

Keywords: nanozymes · nanoceria · peroxidase mimics · transition metals · solid solution

[1] a) T. Montini, M. Melchionna, M. Monai, P. Fornasiero, *Chem. Rev.* **2016**, *116*, 5987–6041; b) K. J. Lee, Y. Kim, J. H. Lee, S. J. Cho, J. H. Kwak, H. R. Moon, *Chem. Mater.* **2017**, *29*, 2874–2882; c) W. Zhan, S. Yang, P. Zhang, Y. Guo, G. Lu, M. F. Chisholm, S. Dai, *Chem. Mater.* **2017**, *29*, 7323–7329; d) A. Primo, T. Marino, A. Corma, R. Molinari, H. García, *J. Am. Chem. Soc.* **2011**, *133*, 6930–6933; e) J. S. Elias, M. Risch, L. Giordano, A. N. Mansour, S. H. Yang, *J. Am. Chem. Soc.* **2014**, *136*, 17193–17200.

[2] a) J. Chen, S. Patil, S. Seal, J. F. McGinnis, *Nat. Nanotechnol.* **2006**, *1*, 142–150; b) B. Liu, Z. Sun, P.-J. J. Huang, J. Liu, *J. Am. Chem. Soc.* **2015**, *137*, 1290–1295; c) M. Soh, D. W. Kang, H. G. Jeong, D. Kim, D. Y. Kim, W. Yang, C. Song, S. Baik, I. Y. Choi, S. K. Ki, H. J. Kwon, T. Kim, C. K. Kim, S. H. Lee, T. Hyeon, *Angew. Chem. Int. Ed.* **2017**, *56*, 11399–11403; *Angew. Chem.* **2017**, *129*, 11557–11561; d) A. Asati, S. Santra, C. Kaittanis, S. Nath, J. M. Perez, *Angew. Chem. Int. Ed.* **2009**, *48*, 2308–2312; *Angew. Chem.* **2009**, *121*, 2344–2348; e) A. A. Vernekar, T. Das, G. Mugesh, *Angew. Chem. Int. Ed.* **2016**, *55*, 1412–1416; *Angew. Chem.* **2016**, *128*, 1434–1438; f) R. W. Tarnuzzer, J. Colon, S. Patil, S. Seal, *Nano Lett.* **2005**, *5*, 2573–2577; g) H. J. Kwon, M. Y. Cha, D. Kim, D. K. Kim, M. Soh, K. Shin, T. Hyeon, I. Mook-Jung, *ACS Nano* **2016**, *10*, 2860–2870; h) Z. Tian, J. Li, Z. Zhang, W. Gao, X. Zhou, Y. Qu, *Biomaterials* **2015**, *59*, 116–124; i) C. Xu, Z. Liu, W. Li, J. Ren, X. Qu, *Adv. Funct. Mater.* **2014**, *24*, 1624–1630; j) X. Liu, W. Wei, Q. Yuan, X. Zhang, N. Li, Y. Du, G. Ma, C. Yan, D. Ma, *Chem. Commun.* **2012**, *48*, 3155–3157.

[3] a) W. Liu, L. Feng, C. Zhang, H. Yang, J. Guo, X. Liu, X. Zhang, Y. Yang, *J. Mater. Chem. A* **2013**, *1*, 6942–6948; b) L. Gao, J. Zhuang, L. Nie, J. Zhang, Y. Zhang, N. Gu, T. Wang, J. Feng, D. Yang, S. Perrett, X. Yan, *Nat. Nanotechnol.* **2007**, *2*, 577–583; c) F. Manea, F. B. Houillon, L. Pasquato, P. Scrimin, *Angew. Chem. Int. Ed.* **2004**, *43*, 6165–6169; *Angew. Chem.* **2004**, *116*, 6291–6295; d) X. Wang, Y. Hu, H. Wei, *Inorg. Chem. Front.* **2016**, *3*, 41–60; e) K. Fan, C. Cao, Y. Pan, D. Lu, D. Yang, J. Feng, L. Song, M. Liang, X. Yan, *Nat. Nanotechnol.* **2012**, *7*, 459–464; f) F. Natalio, R. André, A. F. Hartog, B. Stoll, K. P. Jochum, R. Wever, W. Tremel, *Nat. Nanotechnol.* **2012**, *7*, 530–535; g) G. Y. Tonga, Y. Jeong, B. Duncan, T. Mizuhara, R. Mout, R. Das, S. T. Kim, Y. C. Yeh, B. Yan, S. Hou, *Nat. Chem.* **2015**, *7*, 597–603; h) M. Huo, L. Wang, Y. Chen, J. Shi, *Nat. Commun.* **2017**, *8*, 357–368; i) G. Fang, W. Li, X. Shen, J. M. Perez-Aguilar, Y. Chong, X. Gao, Z. Chai, C. Chen, C. Ge, R. Zhou, *Nat. Commun.* **2018**, *9*, 129–137; j) K. Fan, J. Xi, L. Fan, P. Wang, C. Zhu, Y. Tang, X. Xu, M. Liang, B. Jiang, X. Yan, L. Gao, *Nat. Commun.* **2018**, *9*, 1440–1450; k) X. Shen, W. Liu, X. Gao, Z. Lu, X. Wu, X. Gao, *J. Am. Chem. Soc.* **2015**, *137*, 15882–15891; l) K. Kim Chi, T. Kim, I. Y. Choi, M. Soh, D. Kim, Y. J. Kim, H. Jang, H. S. Yang, Y. Kim Jun, H. K. Park, P. Park Seung, S. Park, T. Yu, B. W. Yoon, S. H. Lee, T. Hyeon, *Angew. Chem. Int. Ed.* **2012**, *51*, 11039–11043; *Angew. Chem.* **2012**, *124*, 11201–11205; m) H. Wei, E. Wang, *Anal. Chem.* **2008**, *80*, 2250–2254; n) J. Hou, M. Vázquez-González, M. Fadeev, X. Liu, R. Lavi, I. Willner, *Nano Lett.* **2018**; o) Q. Wang, X. Zhang, L. Huang, Z. Zhang, S. Dong, *Angew. Chem. Int. Ed.* **2017**, *129*, 16082–16085; p) W. Zhang, S. Hu, J.-J. Yin, W. He, W. Lu, M. Ma, N. Gu, Y. Zhang, *J. Am. Chem. Soc.* **2016**, *138*, 5860–5865; q) J. Yao, Y. Cheng, M. Zhou, S. Zhao, S. Lin, X. Wang, J. Wu, S. Li, H. Wei, *Chem. Sci.* **2018**, *9*, 2927–2933; r) Y. Hu, H. Cheng, X. Zhao, J. Wu, F. Muhammad, S. Lin, J. He, L. Zhou, C. Zhang, Y. Deng, P. Wang, Z. Zhou, S. Nie, H. Wei, *ACS Nano* **2017**, *11*, 5558–5566; s) H. Cheng, L. Zhang, J. He, W. Guo, Z. Zhou, X. Zhang, S. Nie, H. Wei, *Anal. Chem.* **2016**, *88*, 5489–5497; t) J. Sun, Y. Fu, R. Li, W. Feng, *Chem. Mater.* **2018**, *30*, 1625–1634; u) H. Zhao, Y. Dong, P. Jiang, G. Wang, J. Zhang, *ACS Appl. Mater. Interfaces* **2015**, *7*, 6451–6461; v) M. I. Kim, Y. Ye, M. A. Woo, J. Lee, H. G. Park, *Adv. Healthcare Mater.* **2014**, *3*, 36–41.

[4] K. Herget, P. Hubach, S. Pusch, P. Deglmann, H. Götz, E. Gorelik Tatiana, A. Gural'skiy Il'ya, F. Pfitzner, T. Link, S. Schenk, M. Panthöfer, V. Ksenofontov, U. Kolb, T. Opatz, R. André, W. Tremel, *Adv. Mater.* **2016**, *29*, 1603823–1603830.

[5] a) H. Wei, E. Wang, *Chem. Soc. Rev.* **2013**, *42*, 6060–6093; b) Y. Hu, X. J. Gao, Y. Zhu, F. Muhammad, S. Tan, W. Cao, S. Lin, Z. Jin, X. Gao, H. Wei, *Chem. Mater.* **2018**, *30*, 6431–6439; c) D. Jampaiah, T. S. Reddy, A. E. Kandjani, P. Selvakannan, Y. M. Sabri, V. E. Coyle, R. Shukla, S. K. Bhargava, *J. Mater. Chem. B* **2016**, *4*, 3874–3885; d) M. N. Karim, M. Singh, P. Weerathunge, P. Bian, R. Zheng, C. Dekiwadia, T. Ahmed, S. Walia, E. Della Gaspera, S. Singh, R. Ramanathan, V. Bansal, *ACS Appl. Nano Mater.* **2018**, *1*, 1694–1704; e) M. N. Karim, S. R. Anderson, S. Singh, R. Ramanathan, V. Bansal, *Biosens. Bioelectron.* **2018**, *110*, 8–15; f) M. Singh, P. Weerathunge, P. D. Liyanage, E. Mayes, R. Ramanathan, V. Bansal, *Langmuir* **2017**, *33*, 10006–10015.

[6] Y. Li, X. He, J. J. Yin, Y. Ma, P. Zhang, J. Li, Y. Ding, J. Zhang, Y. Zhao, Z. Chai, *Angew. Chem. Int. Ed.* **2015**, *127*, 1832–1835.

[7] H. Cheng, S. Lin, F. Muhammad, Y. W. Lin, H. Wei, *ACS Sens.* **2016**, *1*, 1136–1343.

[8] P. Zhang, H. Lu, Y. Zhou, L. Zhang, Z. Wu, S. Yang, H. Shi, Q. Zhu, Y. Chen, S. Dai, *Nat. Commun.* **2015**, *6*, 8446.

[9] a) C. Yang, X. Yu, P. N. Plessow, S. Heissler, P. G. Weidler, A. Nefedov, F. Studt, Y. Wang, C. Woll, *Angew. Chem. Int. Ed.* **2017**, *56*, 14301–14305; *Angew. Chem.* **2017**, *129*, 14491–14495; b) X. Wang, K. Qian, D. Li, *Appl. Catal. B: Environ.* **2008**, *9*, 2158–2162.

[10] S. Ding, F. Liu, X. Shi, K. Liu, Z. Lian, L. Xie, H. He, *ACS Appl. Mater. Interfaces* **2015**, *7*, 9497.

[11] a) P. Venkataswamy, K. N. Rao, D. Jampaiah, B. M. Reddy, *Appl. Catal. B: Environ.* **2015**, *162*, 122–132; b) C. Korsvik, S. Patil, S. Seal, W. T. Self, *Chem. Commun.* **2007**, *10*, 1056–1058.

[12] a) F. Esch, S. Fabris, L. Zhou, T. Montini, C. Africh, P. Fornasiero, G. Comelli, R. Rosei, *Science* **2005**, *309*, 752–755; b) F. Muhammad, A. Wang, W. Qi, S. Zhang, G. Zhu, *ACS Appl. Mater. Interfaces* **2014**, *6*, 19424–19433; c) M. Singh, D. Jampaiah, A. E. Kandjani, Y. M. Sabri, E. Della Gaspera, P. Reineck, M. Judd, J. Langley, N. Cox, J. van Embden, E. L. H. Mayes, B. C. Gibson, S. K. Bhargava, R. Ramanathan, V. Bansal, *Nanoscale* **2018**, *10*, 6039–6050.

[13] R. Cai, D. Yang, S. Peng, X. Chen, Y. Huang, Y. Liu, W. Hou, S. Yang, Z. Liu, W. Tan, *J. Am. Chem. Soc.* **2015**, *137*, 13957–13963.

Manuscript received: September 27, 2018
Revised manuscript received: October 28, 2018
Accepted manuscript online: October 29, 2018
Version of record online: December 4, 2018